Tribology International 164 (2021) 107240

Contents lists available at ScienceDirect

Tribology International

journal homepage: www.elsevier.com/locate/triboint

Development of white etching bands under accelerated rolling contact fatigue

Muhammad U. Abdullah [a], Zulfiqar A. Khan [a,*], Wolfram Kruhoeffer [b], Toni Blass [c], Bernd Vierneusel [c]

[a] Bournemouth University, Department of Design & Engineering, NanoCorr, Energy & Modelling (NCEM) Research Group, Poole, Dorset, United Kingdom
[b] Schaeffler Technologies AG & Co. KG, Herzogenaurach, Germany
[c] Schaeffler Technologies AG & Co. KG, Schweinfurt, Germany

ARTICLE INFO

Keywords:
rolling contact
white etching bands
bearing elements
4-ball test
diffusion

ABSTRACT

Bearing steel under severe loading condition undergoes substantial subsurface microstructural alterations known as Dark etching regions and white etching bands. White etching bands (WEBs) develop after hundreds of millions of stress cycles in bearing components and have been reported for several decades but the formation mechanism of white bands is not fully elucidated. Current research presents a systematic rolling contact fatigue (RCF) testing in a rotary tribometer under accelerated conditions, where rolling cycles are simulated in a 4-ball test configuration. The post RCF investigations have been carried out to understand the formation mechanism of WEBs in a ball-on-ball point contact load. WEBs have been characterised with the help of nanoindentation and Energy-dispersive X-ray spectroscopy analysis. The quantitative analysis of WEBs growth with subsurface stress field has revealed that the unique orientations of white bands are governed by the plane of maximum relative normal stress along the contact track. Moreover, the accelerated growth and reversal of WEBs sequence at elevated temperature have revealed that the WEBs formation is dependent on temperature/load combination. The observed growth of lenticular carbides in current research is also compared with dislocation gliding model and the role of carbon diffusion within WEBs is highlighted.

1. Introduction

Bearing elements manifest rolling contact fatigue (RCF) resulting in irreversible subsurface microstructural alterations, when loaded beyond yield strength. The different feature microstructures, mainly dark etching regions (DERs) and white etching bands (WEBs), are visible under the microscope after Nital etching. It is believed that such microstructural alterations are developed due to the decay of parent martensitic structure and microstructural phase transformations during multiaxial stress histories of RCF [1,2].

The WEBs appear as white bands in bright field microscopy and are typically observed after hundreds of millions of stress cycles during nominal operating conditions with a threshold limit above yield point [3,4]. WEBs are formed as parallel thin plates which are oriented parallel and inclined to the rolling direction as observed in the axial and circumferential cutting plane and are reported with/without the presence of DERs. WEBs consist of carbon-rich and carbon depleted areas which are known as lenticular carbides (LCs) and ferrite bands [5,6]. It has been reported in [5] that lenticular carbides and ferrite bands represent localised soft and hard regions as compared to parent microstructure. This hardness fluctuation of WEBs manifests carbon redistribution during RCF, however, the variation of localised hardness within WEBs is not reported so far.

WEBs are further categorized as lower angle bands (LABs) and higher angle bands (HABs) due to their unique orientations with the rolling direction. The LABs are usually oriented at 20°–35° whereas the HABs are oriented at steeper angles of 65°–85° with the surface [6]. The thickness and length of LABs are reported as 0.5 μm and 5–30 μm whereas for HABs it is 10 μm and up to 100 μm respectively [1,5,7]. The morphology of WEBs has been reported as a thin plate which grows in space (i.e., length, width, and thickness) as well as in density. More recently, a three-dimensional representation of a HABs/LABs has been reported in [8,9] by serial sectioning of bearing steels. The results showed that the HABs develop at the saturated and dense regions of LABs and such bands formation accelerates at high contact pressure. Contrary, Mitamura et al. [10] has reported development of HABs prior

* Corresponding author.
E-mail address: zkhan@bournemouth.ac.uk (Z.A. Khan).

https://doi.org/10.1016/j.triboint.2021.107240
Received 18 May 2021; Received in revised form 6 August 2021; Accepted 18 August 2021
Available online 20 August 2021

Table 1
Composition of AISI-52100 bearing balls (in weight %).

C	Mn	P	S	Si	Cr	Ni	Cu	Mo	Al	O
		(max)	(max)			(max)	(max)		(max, total)	(max)
0.93–1.05	0.25–0.45	0.025	0.015	0.15–0.35	1.35–1.60	0.25	0.30	0.10	0.050	0.0015

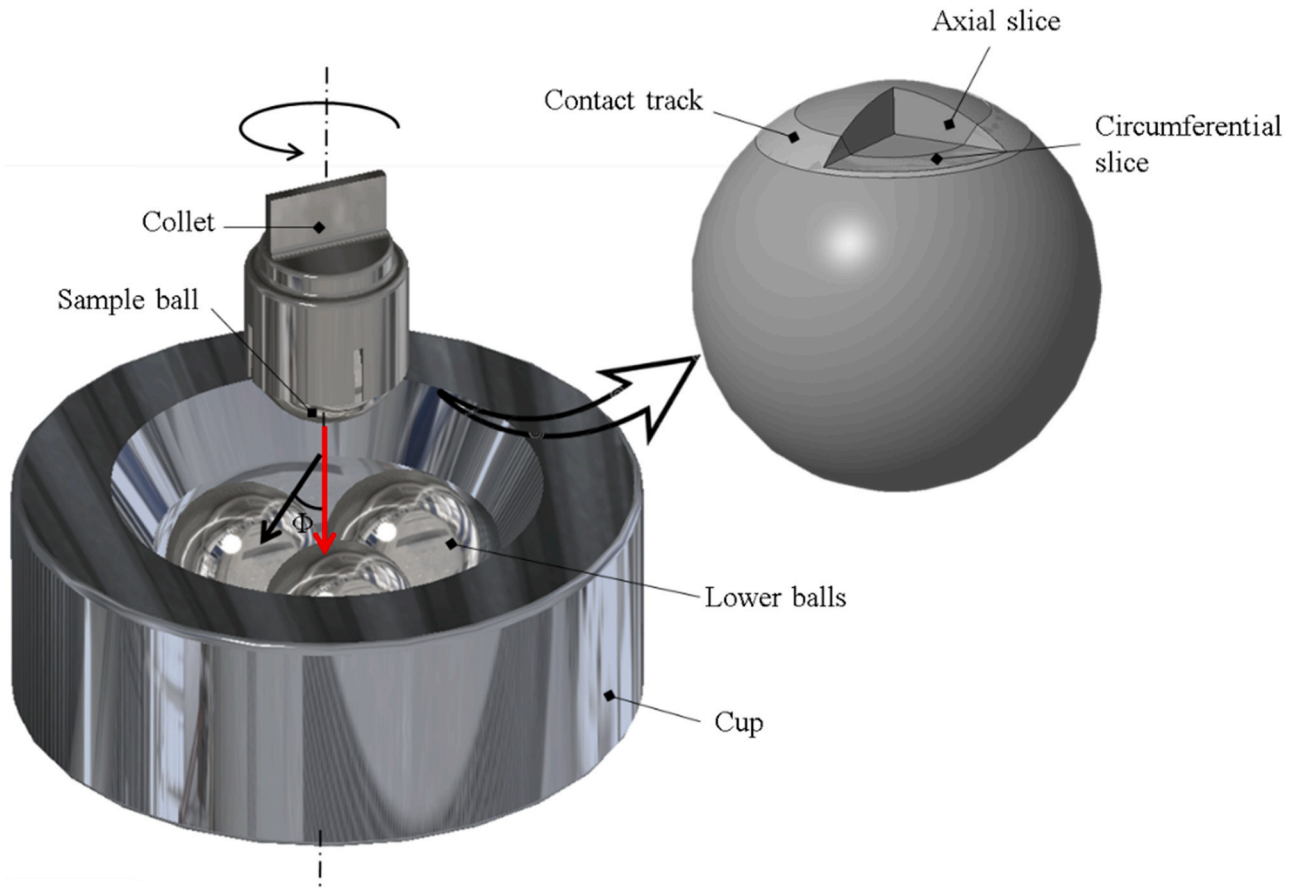

Fig. 1. Schematic for 4-ball test conducted in a rotary tribometer. The applied axial load makes an angle $\Phi = 35.25^{\circ}$ with the resultant load, represented by red and black load vectors, respectively. The axial and circumferential orientations for subsurface investigations are also illustrated. For interpretation of the references to color in this figure legend, the reader is referred to the web version of this article.

to LABs at high contact pressure. It was suggested that a contact stress as high as 4.8 GPa can result in the favourable formation of HABs, however it was not explained which factors drive the early formation of HABs.

The causes for the formation of WEBs are discussed differently in literature. Studies in [4,11] reported WEBs to be stress induced and as a result of subsurface plastic deformation. It was also suggested in [12] that the structural changes during RCF develop due to recrystallization where carbon atoms diffuse from supersaturated regions of ferrite to form LCs. Other explanations in [10,13,14] are based on the fact that energy is required to generate the interstitial diffusion of carbon from ferrite to LCs. This activation energy was associated with the dissipated plastic energy. Another theory in [12] suggested dislocation annihilation as a source of carbon depletion in the ferrite bands. More recently, a dislocation gliding based carbon migration theory has been presented by Fu et al. [15] which stated the carbon diffusion from ferrite bands to thicken the adjacent lenticular carbides. Nevertheless, all these theories focus on the carbon migration governed by diffusion or plastic deformation. Although there is broad consensus in the literature that carbon migration plays a central role in rolling contact fatigue [3,12,16], a clear understanding is still needed to elucidate the ambiguities regarding the formation and orientation of white bands.

The current research is studying the development of white bands formation under controlled/accelerated loading conditions. For RCF testing, a rotary tribometer has been used with 4-ball test configuration to conduct pure rolling cycles on a bearing ball. After the test, subsurface microscopic analysis has been conducted for possible white bands formation. The novelty of current research relies on the postulate that WEB formation mechanisms is yield controlled (and not stress controlled as suggested by previous publications). The order of appearance for feature microstructure in current research is formation of DER followed by the development of LABs and HABs at 100 °C operating temperature whereas at elevated temperature (160 °C) the HABs proceed LABs. For white bands characterisation, nanoindentation and SEM/EDS analysis results are also included in Section 4.

2. Experimental details

2.1. Materials

For RCF testing, a standard martensitic heat-treated AISI-52100 (designation according to ISO 683-17 is 100Cr6) with 12.7 mm diameter bearing balls have been used. During manufacturing, tumbling was avoided to exclude the effects of mechanical residual stresses. The residual stresses from surface finishing of the balls are not significant as

Table 2
Four ball experiments.

Test Id.	Max. Hertzian contact pressure (GPa)	Operating temperature (°C)	Speed (rpm)	Stress cycles
1	6	100 °C	9100	22×10^6
2		100 °C		37×10^6
3		100 °C		55×10^6
4		160 °C		22×10^6
5		160 °C		37×10^6
6		160 °C		55×10^6
7		160 °C		100×10^6

they are only limited to 5–10 μm from the surface. The resultant material has a typical needle-like microstructure containing 10–11% retained austenite along with primary carbides $(Fe,Cr)_3C$ [17] and its chemical composition is listed in Table 1.

2.2. Testing

RCF testing was conducted in a programmable high-speed rotary tribometer with 4-ball test configuration. The tested sample ball is fixed in a collet which then rotates on top on lower three balls which are free to roll in a cup, as shown in schematic Fig. 1. One complete rotation of upper ball exerts 2.25 stress cycles and resulting in a contact track shown on the right in Fig. 1. A standard grade synthetic oil ISO-VG-320 was used as a bath lubricant enabling a full film lubrication to avoid asperities interaction of ball samples. The temperature was monitored continuously by a K-type thermocouple installed in the cup housing and was kept constant before each test to normalise the testing conditions. Further details of ball samples (hardness, surface roughness) and lubrication condition can be found in author's previous work [18]. Once the required stress cycles were obtained, the test was suspended, and the upper sample ball was sliced in axial (perpendicular and in the middle of contact track) and circumferential plane (parallel to contact track). A complete set of experiments are available in Table 2. After careful sample preparation, a 3% Nital etchant was used to reveal possible microstructural alterations. An optical interferometer was also employed to measure the deformed contact track profile after RCF testing.

3. Results

3.1. White etching bands

The optical images obtained from the post RCF microscopic investigations are shown in Figs. 2 and 3. Fig. 2 represents the subsurface micrographs of axial and circumferential sliced samples obtained at 6 GPa contact pressure, 100 °C lubricant temperature with 22, 37 and 55 million stress cycles. It can be observed that the formation of DERs is accompanied by the development of white etching regions after 22 million cycles as indicated in Fig. 2(a). This white etching region is bounded by the upper and lower boundaries of DER, observed in the circumferential and axial sliced sample. This white region comprises LABs, oriented parallel to the surface in axial slice and 30° to the rolling direction (RD) in circumferential slice. The density and size of LABs can be observed to increase with progressive RCF cycles. A highly saturated region of LABs can be seen in the inset of Fig. 2(b) where a closely packed LABs structure is visible. With increase in LABs density, another set of white bands start to form and are termed as HABs. These bands make ~75° with the surface and can be observed after 55 million stress cycles as observed in Fig. 2(c).

Earlier studies [3,8,19] have reported that the HABs are formed due to the shear breakdown of LABs during RCF loadings. The formation of HABs in the close proximity of pre-existing LABs make it difficult to observe in the bright field microscopy where boundaries of LABs and HABs diffuse with each other. A recent study [8] has shown that LABs can be distinguished from HABs in a deep etched sample with the use of a polarized light due to variance in morphology and uniquely oriented grains structure. The contrast images obtained from cross-polarized light indicate the unidirectional grain structure of WEBs. The distinctive features of the LABs and HABs can be seen with the help of a cross polarized light in Fig. 2(c).

It can be observed that LABs start to disappear with the formation of HABs, indicating the breakdown of LABs as a prerequisite for HABs growth at 6 GPa and 100 °C operating temperature. The results reported for HABs and LABs are in good agreement with the literature for white bands formation under typical operating temperatures. Slight variations in the characteristic of the bands can be observed due to the difference in contact geometries. Most of the reported data for white bands formation is acquired from the inner ring of bearing components which is quite different from ball-on-ball point contact load in 4-ball testing presented in current research. Additionally, deep groove ball bearing usually operate with up to 5–10% slip [20] whereas current study relies on the pure-rolling cycles in a 4-ball test ensuring no contact of asperities.

Recent studies [18,21] have reported that the development of WEBs is associated with the accumulated plastic strain, therefore an enhanced formation of WEBs would be expected at elevated operating temperatures due to lowering of yield stress. Fig. 3 represents the subsurface micrographs of RCF tested samples at 6 GPa with 160 °C operating temperature. It can be seen in Fig. 3(a) that an early formation of HABs is observed just after 22 million cycles. The inset of this figure shows that HABs developed without any LABs formation. It can be postulated that the elevated operating conditions have resulted in sever plastic deformation leading directly to HABs formation. It has been reported [10,22] that the predominate formation of HABs prior to LABs can be seen after a threshold contact stress of 4.6 GPa. In this study, the applied contact stress in 6 GPa where LABs are observed before HABs at 100 °C whereas a reversal of sequence of WEBs formation can be seen at 160 °C. This indicates that no stress threshold exists for prior formation of steeper bands, and it appears to be associated with applied temperature and load combination which in turn affect subsurface plasticity. Nevertheless, understanding the reversal of sequence of WEBs appearance would require further investigations and can be addressed in future work.

It should be noted that the orientation of WEBs observed in circumferential sliced RCF tested samples are slightly different than the true orientation with the contact track. This is because of the unique loading mechanism of 4-ball test where the resultant load between upper ball and lower ball in contact makes an angle of $\Phi = 35.26°$ with axially applied load, refer to Fig. 1. The continuous varying plane of applied load in bearing balls during 4-ball test configuration makes it difficult to reveal the microstructure in a true parallel plane which varies continuously along the contact track. For investigation ease, the RCF tested samples are sliced in an alternative circumferential plane and axial plane as demonstrated in Fig. 1. Both axial and circumferential sections reveal a 3d microstructure of WEBs which can be characterised and transformed. From the knowledge of cutting plane and observable features found in respective slices, a CAD model can be generated to interpret the three-dimensional structure of WEBs and its unique orientations in three-dimensional space. The features of HABs can be defined with the measured length, thickness (observed in true parallel slice) and span (observed in axial slice) of the band. The typical characteristic of LABs, HABs and sLABs found during microscopic analysis are listed in Table 3.

With increasing stress cycles, a noticeable growth in HABs can be seen in Fig. 3(c) where HABs appear thicker and lengthened. A white band constitutes a ferrite band sandwiched between carbon-rich plates, known as lenticular carbides (LCs) [5,19]. With an increase in stress cycles, the length, thickness, and span of HABs increases whereas the spacing between adjacent bands decreases. This WEBs growth has been defined as density of WEBs per unit area and is expressed as WEB% [15]. Additionally, the WEBs can also be characterised by the rate of

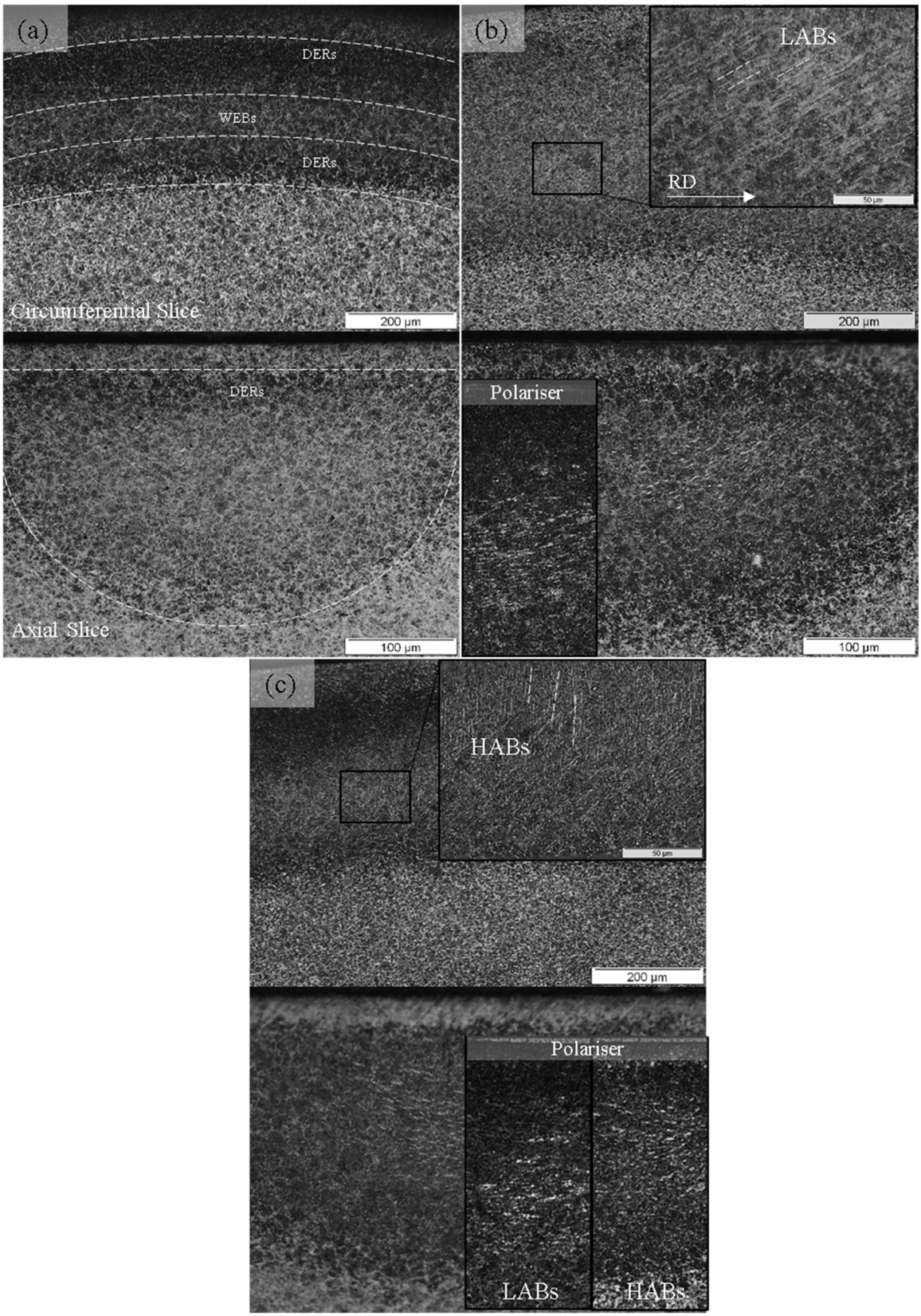

Fig. 2. Subsurface investigation of RCF tested samples at 6 GPa contact pressure with 100 °C lubricant temperature after (a) 22 million (b) 37 million and (c) 55 million cycles. Top and bottom rows represent circumferential and axial slices respectively. Images are scaled to same size.

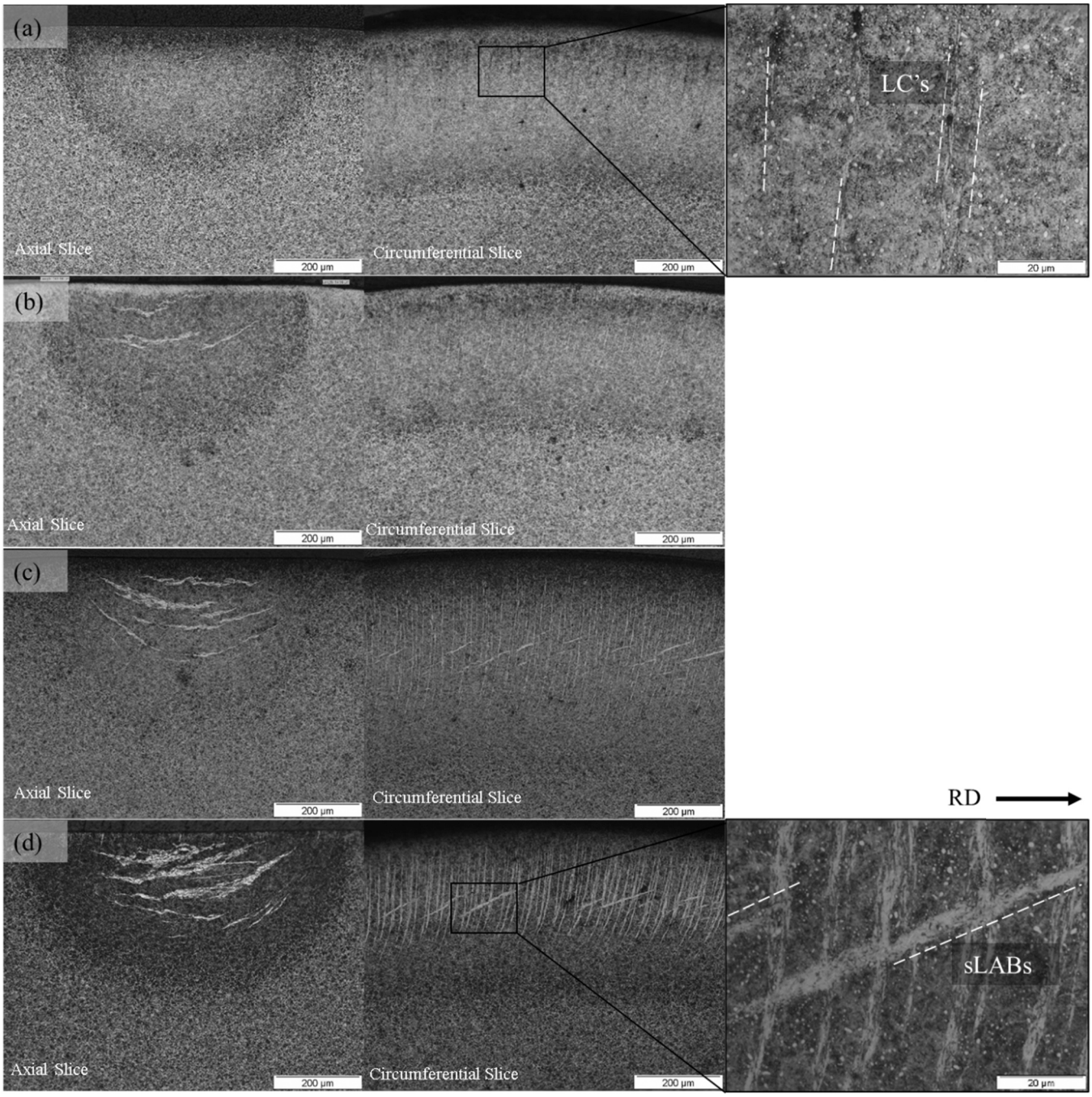

Fig. 3. Subsurface investigation of RCF tested samples at 6 GPa contact pressure and 160 °C lubricant temperature after (a) 22 million, (b) 37 million, (c) 55 million and (d) 100 million cycles.

thickening of LCs which are observed along the boundaries of ferrite bands. Fig. 3(c) and 3(d) represents the micrographs obtained after 55 million and 100 million cycles where distinctive oriented lower angle bands start to appear and grow with progressive stress cycles and are termed as secondary lower angle bands (sLABs). These sLABs appear on top of pre-existing white bands, and the depth range of these bands lies closer to the nucleation sites of HABs. The early formation of HABs and later development of sLABs have been reported earlier by [10,22], however, the comparison of the current study with the literature is limited due to differences in contact mechanics of 4-ball test with the bearing inner ring. The current study employs RCF testing under pure rolling with accelerated testing conditions where the subsurface microstructural alterations have been observed in reasonable testing time.

As discussed earlier, the microscopic analysis conducted on the circumferential sections does not reveal the true nature orientation of WEBs where the results were transformed to obtain the characteristic lengths of WEBs. Following extensive microscopic investigations, a full-scale WEBs representation under ball-on-ball point contact load is presented in Fig. 4. The unique orientation of white bands along with spacing and extent can be observed in the circumferential plane and axial plane. Any slight misorientation in the sample preparation would result in deviation of observed WEBs as observed in the micrographs of axial slice sample. Additionally, the predicted characteristics of WEBs in the true parallel slice can be compared with the respective micrograph which can reveal the true orientation of distinctive white bands.

Table 3
Characteristics of WEBs observed in ball-on-ball RCF testing.

Feature microstructure	Lower angle bands (LABs)	Higher angle bands (HABs)	Secondary lower angle bands (sLABs)
Current study			
Spacing (μm)	5–6	10–40	50
Length (μm)	8–20	120–150	95–141
Angle	25°–30°	70°–78°	16°–20°
Thickness (μm)	1–2	5–7	5–8
Span length (μm)	10–22	150–180	132–151
Structure	–	Ferrite sandwiched with LCs	Ferrite
Literature [5,8,10,22–24]			
Spacing (μm)	0.5–10	5–50	–
Length (μm)	5–30	100	–
Angle	20–35°	65°–85°	20°–25°
Thickness (μm)	0.1–2	10	–
Structure	Ferrite with dissolved carbides	Pure ferrite	Ferrite with high dislocation density

The microstructure of WEBs and its development in various stages of RCF is shown in Fig. 5. For electron microscope analysis, samples have been polished with 0.25 μm diamond suspension and slightly etched to reveal microstructure. Fig. 5(a) represents the parent microstructure of an untested sample, and Fig. 5(b) represents the micrograph of LABs obtained at 6 GPa, 100 °C after 37 million cycles. The microstructure reveals equiaxed ferrite band formation within the martensitic matrix which ranges from 10 to 22 μm in span. Around the boundaries of deformed ferrite bands, formation of elongated carbide structure (LCs) can be observed as indicated with red arrows. The nucleation and growth of LCs is accompanied by breakdown of primary θ carbides along the plane of ferrite band as highlighted with white arrow. Šmeļova et al. [5], after electron microscopic analysis of fatigue tested bearing inner ring, has reported that the ferrite bands contain equiaxed ferrite grains where the LCs grow along the boundaries of ferrite and its thickness increase with progressive stress cycles. The growth of LCs is associated with the diffusion of carbon atoms in ferrite. In order to drive this carbon, significantly high energy is required, particularly to dissolve pre-existing carbides. This activation energy has been cited to be from the dissipated plastic energy during RCF induced subsurface plasticity [10]. Additionally, Fu et al. [15,21,25] has suggested that the formation of LCs is governed by the rearrangement of crystal structure and dislocation gliding. It is suggested that dislocation motion during RCF assist in transport of carbon atoms to precipitates at the boundaries of heavily deformed ferrite. Additionally, after considerable rolling cycles (substantial plasticity), the heavily deformed ferritic region becomes supersaturated with carbon, where carbon can segregate at dislocation sites forming carbon-rich plates with concentration as high as primary carbides. The growth of LCs continues till the carbon concentration in the ferrite bands reaches the equilibrium concentration.

Fig. 5(c), (d) & (e) represents the circumferential micrograph obtained at 6 GPa with 160 °C operating temperature. At such elevated temperatures, an enhanced formation of HABs is observed which contains elongated ferrite bands. The presence of enhanced elongated ferrite bands just after 37 million cycles shows the substantial plasticity accumulated causing martensite to ferrite transformation. The ferrite bands, represented with white-capped lines, are surrounded by the carbide plates which appear at the boundaries of ferrite. A complete dissolution of carbides within ferrite bands can be observed.

After 55 million cycle, Fig. 5(d), the carbides plates appear thicker, ~1 μm which shows that LCs not only grow across boundaries of ferrite, but their thickness also increase. A unique oriented secondary lower angle bands (sLABs) appear in the vicinity of HABs. These elongated

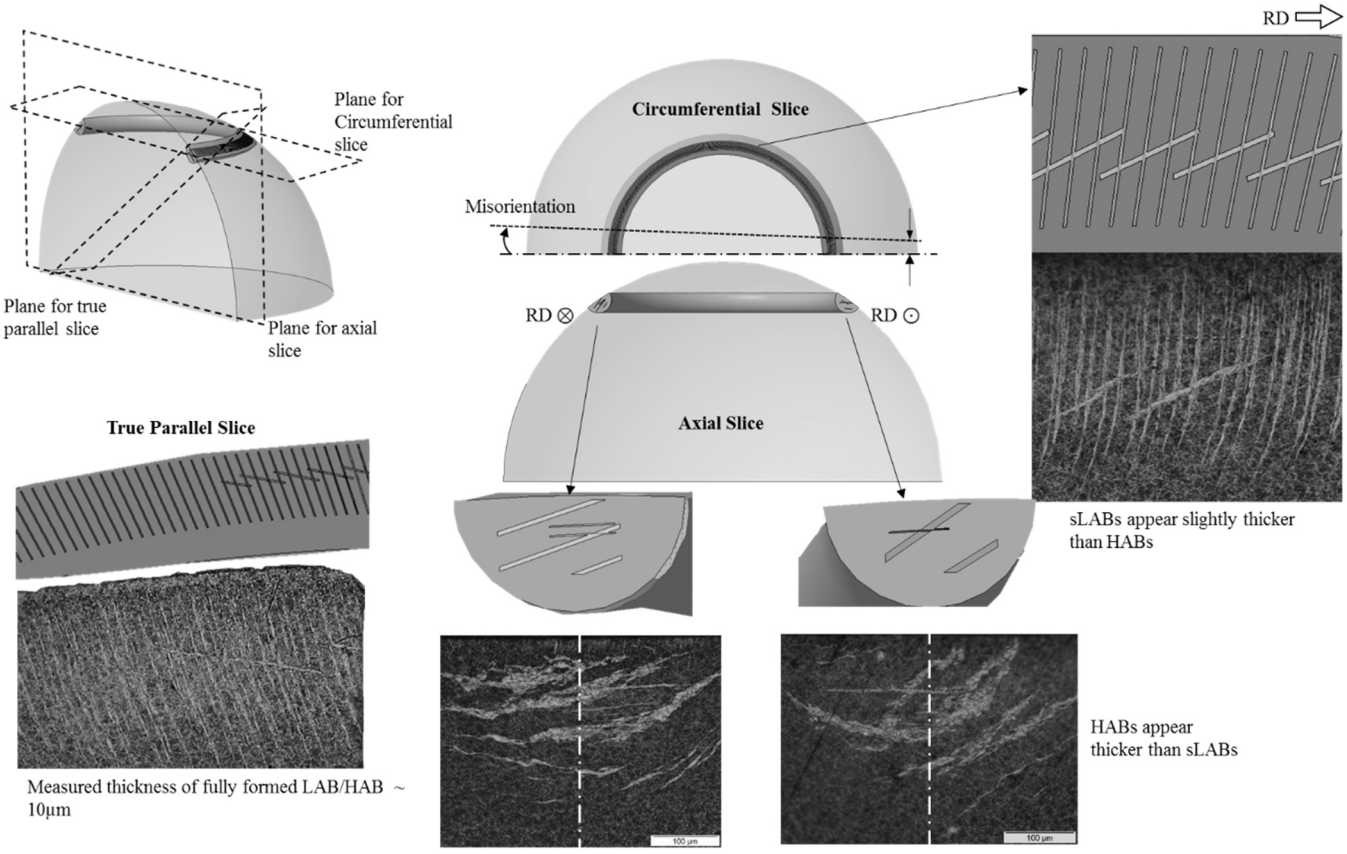

Fig. 4. A full-scale 3d representation of WEBs developed in ball-on-ball point contact load.

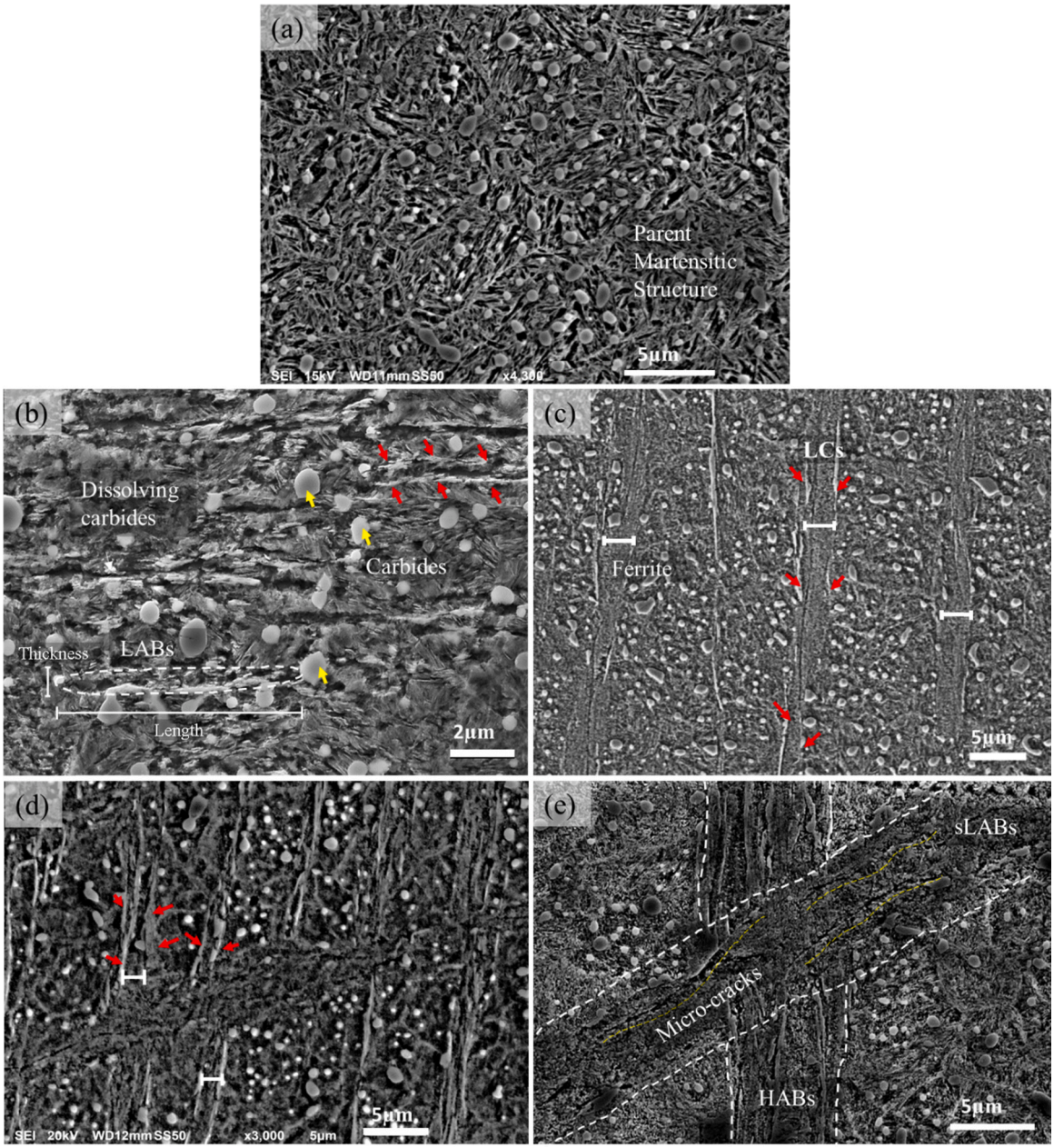

Fig. 5. Parent structure is shown in (a). Development of WEBs in different stages of RCF represented in axially sliced sample (b) after 37 million cycles at 100 °C and circumferential sliced sample after (c) 37 million cycles at 160 °C (d) 55 million cycles at 160 °C (e) 100 million cycles at 160 °C. Red arrows represent the lenticular carbides observed around ferrite bands shown with white-capped line, yellow dotted line represents growth of crack within WEBs whose boundaries are marked with white dashed lines. For interpretation of the references to color in this figure legend, the reader is referred to the web version of this article.

band like structure form at the shear breakdown of HABs, where the boundaries of HABs are dissolved within the ferritic region of sLABs. As indicated in Figs. 2 and 3 that the depth range of sLABs coincides with the nucleation sites of HABs. Additionally, the sLABs grow at the fully saturated regions of HABs and appear as a heavily deformed ferrite band. It is suggested that the development of sLABs requires the dissolution of pre-existing HABs, causing its shear breakdown as indicated in Fig. 5(e). The growth of sLABs can be observed from 55 to 100 million stress cycles. Moreover, these bands contain microcracks which propagate along the plane of bands orientation. It is plausible for cracks to appear and grow at the region softer than the surrounding matrix. To understand the formation mechanism of WEBs, the localised change in hardness and characterisation of newly formed bands become crucial and will be discussed in coming sections.

The chemical redistribution within WEBs is presented in Fig. 6 with the help of energy-dispersive X-ray spectroscopy (EDS) analysis. A region of interest containing HABs and sLABs is selected for EDS analysis and shown in Fig. 6(a) and (b) after Nital etching. The distribution of carbon and chromium is shown in Fig. 6(c) and (d) along with the EDS spectrum of detected elements in Fig. 5(e). The carbon and chromium maps indicate the chemical redistribution of respective elements during WEBs formation. The dissolution of primary carbides ($(Fe,Cr)_3C$) within HABs is obvious due to the reason that chromium is redistributed within HABs. Additionally, no segregation of chromium can be observed within the HABs. Whereas areas of ferrite appears carbon depleted surrounded by the areas of lenticular carbides validating that later stage fully saturated HABs contains ferritic regions along with lenticular carbides clusters where carbon has been segregated from ferritic regions to the adjacent LCs. In addition, the sLABs appear carbon depleted, where intact carbides and dissolved carbides can be observed in Fig. 6(a). The

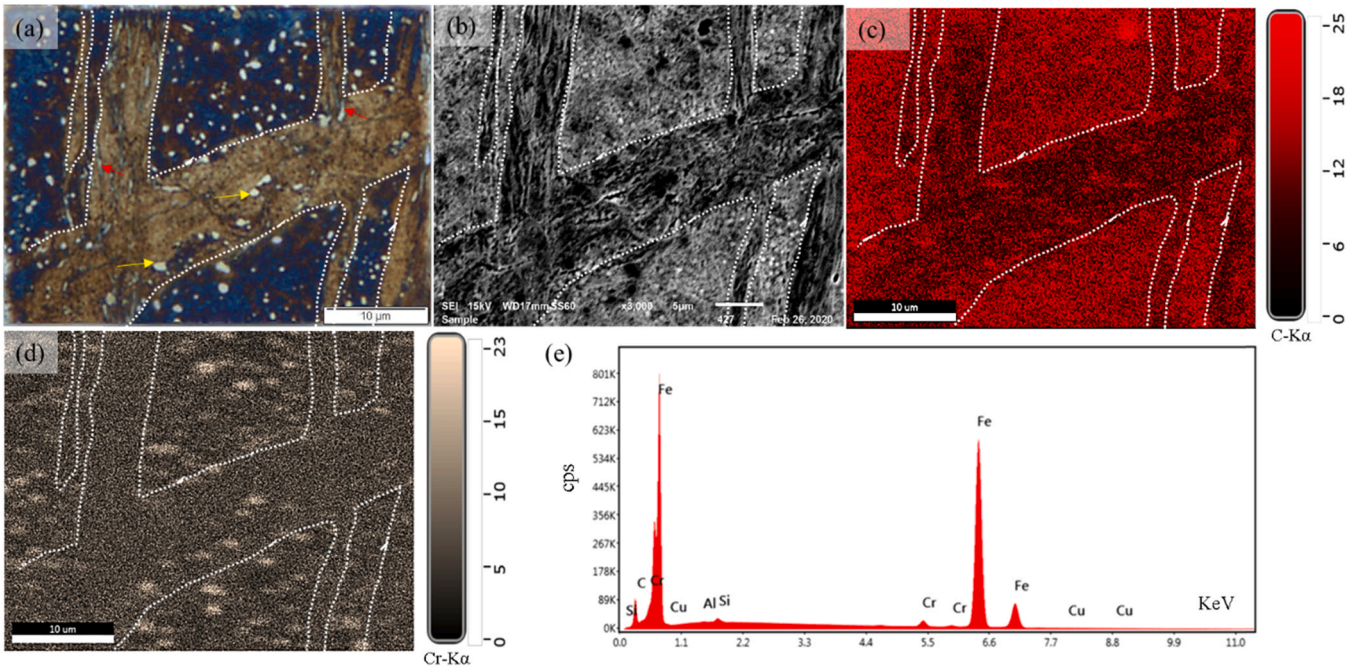

Fig. 6. (a), (b) Etched micrographs revealing sLABs and HABs; (c), (d) & (e) represents EDS analysis for area region shown in (a). Yellow marks represent intact carbides and red marks represents dissolved carbides. The boundaries of WEBs have been masked from optical micrographs and highlighted in EDS mapping with white dotted lines. For interpretation of the references to color in this figure legend, the reader is referred to the web version of this article.

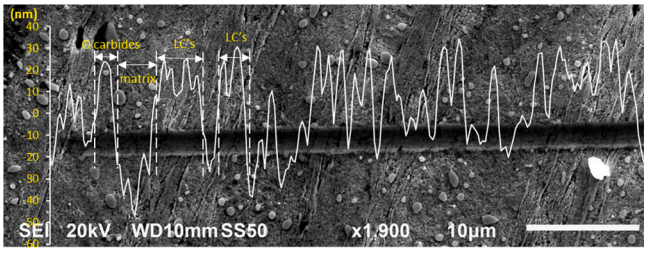

Fig. 7. LCs morphology obtained from a nanoindenter multipass topography test.

boundaries of WEBs marked with white dotted lines in Fig. 6(b), highlights the white band containing the ferritic region along with the corresponding LCs. It should be noted that the carbon and chromium maps from EDS represents a qualitative analysis which represents depletion of carbon within WEBs. A fairly high depletion of carbon can be observed in sLABs representing a pure ferritic nature, whereas the regions of HABs constitute clusters of LCs and ferrite.

3.2. Bands morphology

To reveal the WEBs morphology, a sample was polished with 0.025 µm Alumina suspension and etched with Nital solution for 6–10 s. The resultant etched surface is investigated with a multipass topographic investigation using a 5 µm conical nanoindenter. A 0.1mN load is applied in the first pass to acquire the surface profile of 60 µm horizontal distance on an etched circumferential sliced RCF tested sample as shown in Fig. 7.

To mark the start and endpoint of initial investigated path, a second pass is run where the nanoindenter tool travels with 50mN load creating a wear scar which can be seen in form of a scratch. Comparing the first pass topographic results with the SEM image, the primary carbides and lenticular carbides appear as peaks whereas the ferritic regions along with the parent matrix appear as deep valleys. The topographic results for HABs morphology confirm that the later stage fully developed HABs exist in form of a cluster of LCs and show strong resistance to Nital etching as compared to the surrounding matrix and sandwich ferrite regions. Additionally, from Fig. 7, it can be observed that the resistances to Nital etching of the microstructural features in the material, which are determined by their chemical properties, follow such a sequence: primary θ-carbides > LCs > ferrite bands, which follows the descending trend of carbon content in these features.

3.3. Hardness mapping

As presented above, later stage HABs are made up of thin plates of lenticular carbides which consumes carbon from the nearby ferrite regions. The redistribution of carbon within white bands results in areas of hardening and softening. This localised change in hardness change for white bands is reported in Fig. 8 with two regions of interests (ROIs) for nanoindentation analysis as shown. A Berkovich indenter was employed to perform hardness mapping on the areas of WEBs. A suitable load was applied with a 5 s dwell time and fixed time load/unload of 10 s.

The ROI:1, Fig. 8(a), shows hardness mapping for HABs surrounded by altered martensitic matrix. It is evident that the HABs shows a significantly higher hardness of 10–11 GPa whereas the unaltered microstructure shows a hardness of ~9 GPa. The change in hardness for HABs satisfies the morphology analysis which showed that LCs and primary carbides show strong resistance to Nital etchant. A more detailed hardness mapping can be seen in ROI:2, Fig. 8(b). It can be observed that the maximum hardness for lenticular matches with the hardness of the primary carbides in the matrix and is found as high as 11 GPa as observed from hardness mapping. The higher hardness of HABs suggests an enhanced formation of carbon-rich plates in the later stages of RCF where LCs grow within the regions of ferrite and in this case locally form a cluster in the area where the hardness indentations were placed.

Additionally, another region of softening can be observed in the zones of sLABs, highlighted with white dash-dot lines with a decrease in hardness of 1.5 GPa (141 HV). A recent study [5] has reported a similar decrease in nanohardness in the ferritic regions of white bands where a hardness as low as 4–6 GPa was reported. Moreover, for carbon enriched

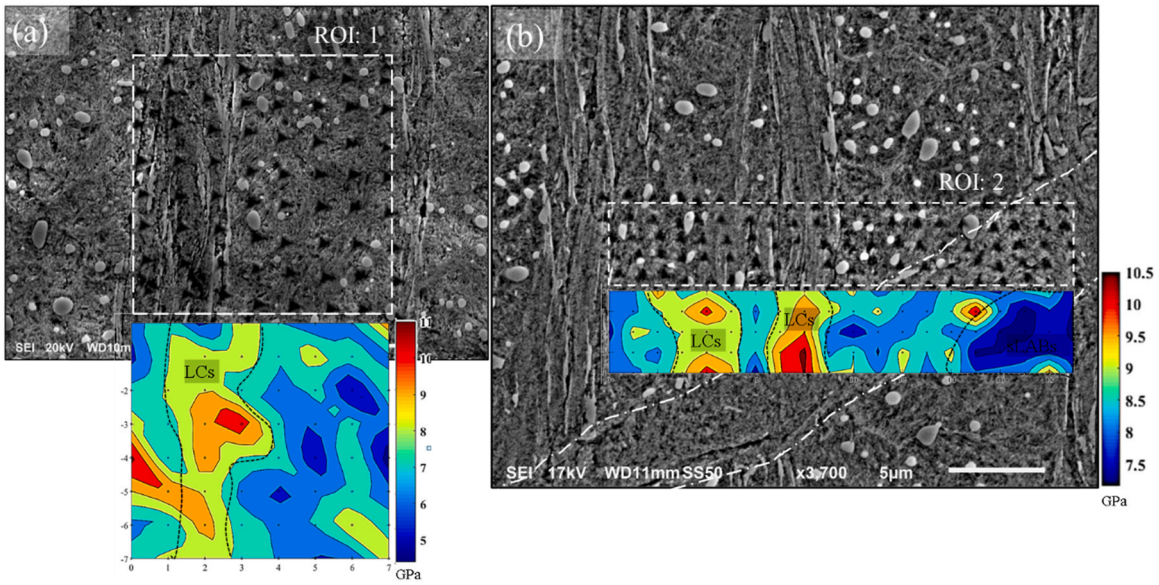

Fig. 8. Hardness mapping of WEBs with nanoindentation. (a) and (b) represent hardness mapping for ROI:1 and ROI:2 respectively. The regions of LCs and sLABs have been marked with black dotted lines.

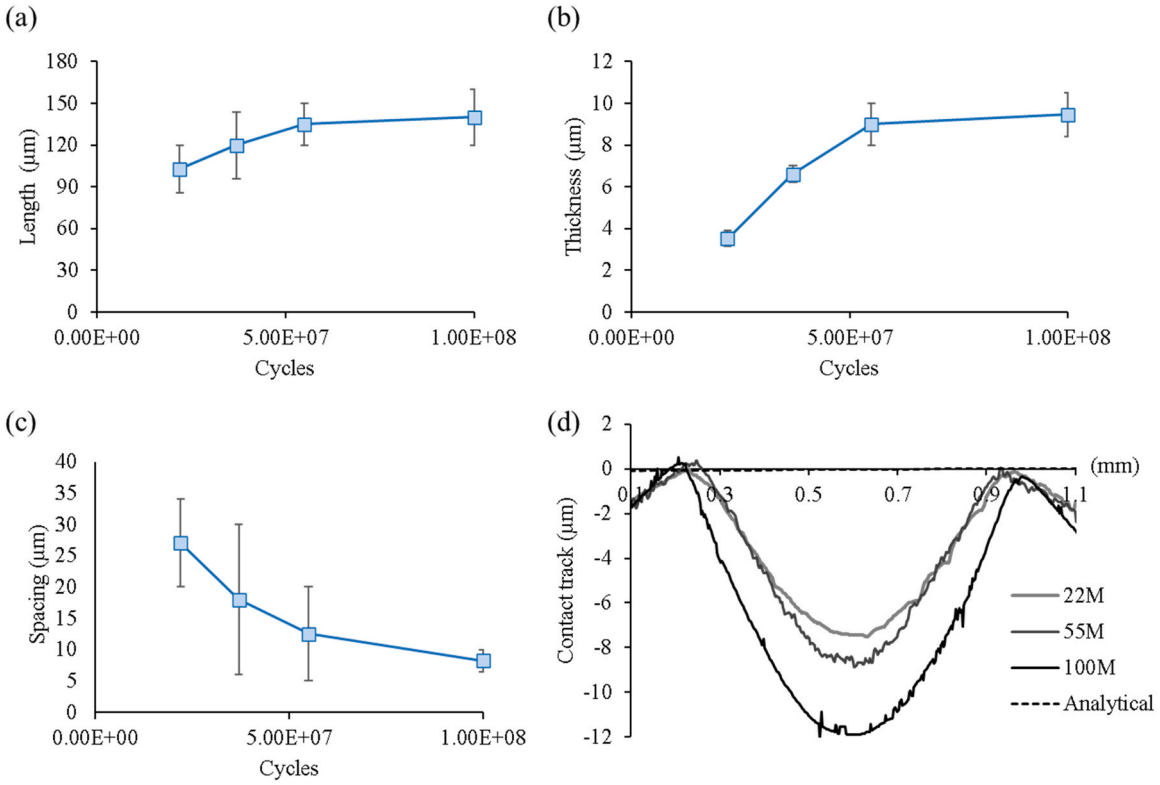

Fig. 9. (a), (b), (c) represents growth of WEBs with change in length, thickness and spacing of HABs with elapsed stress cycles; (d) shows contact track plasticity.

areas, the reported hardness was found in the range of 10–11 GPa. The change in localised hardness within WEBs can be explained by considering the redistribution of carbon, crystallinity, and grain structure.

4. Discussions

4.1. WEBs growth

The development and growth of WEBs with continuous stress cycles, as reported in Section 3, has been reported in earlier research work. It has been believed that the formation mechanism of white bands is stress-controlled where a high stress accelerates the initiation and progression of WEBs. However, it has been debatable which stress component is responsible for microstructural alterations. In Section 3, it has been reported that an enhanced formation of WEBs is observed at elevated operating temperatures i.e., at 160 °C. Hence, it can be postulated that formation mechanism of WEBs is yield controlled where a high yielding resulting from an elevated operating condition result in accelerated

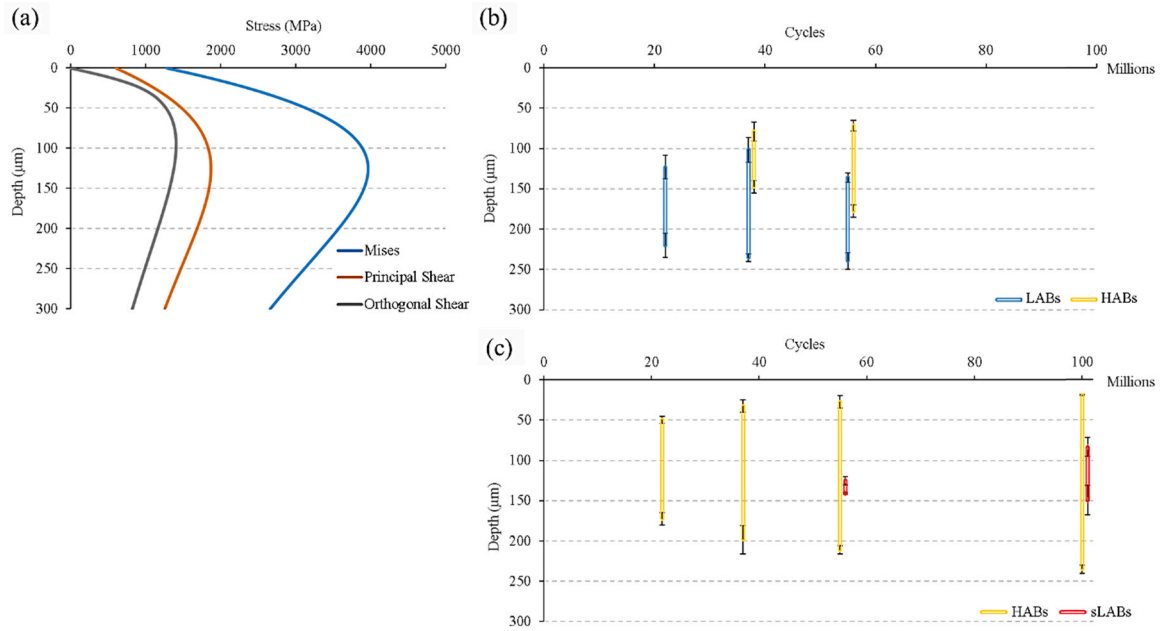

Fig. 10. (a) Subsurface stress distribution at 6 GPa contact pressure; (b) and (c) Development of WEBs plotted as a function of depth and rolling cycles at 100 °C and 160 °C respectively.

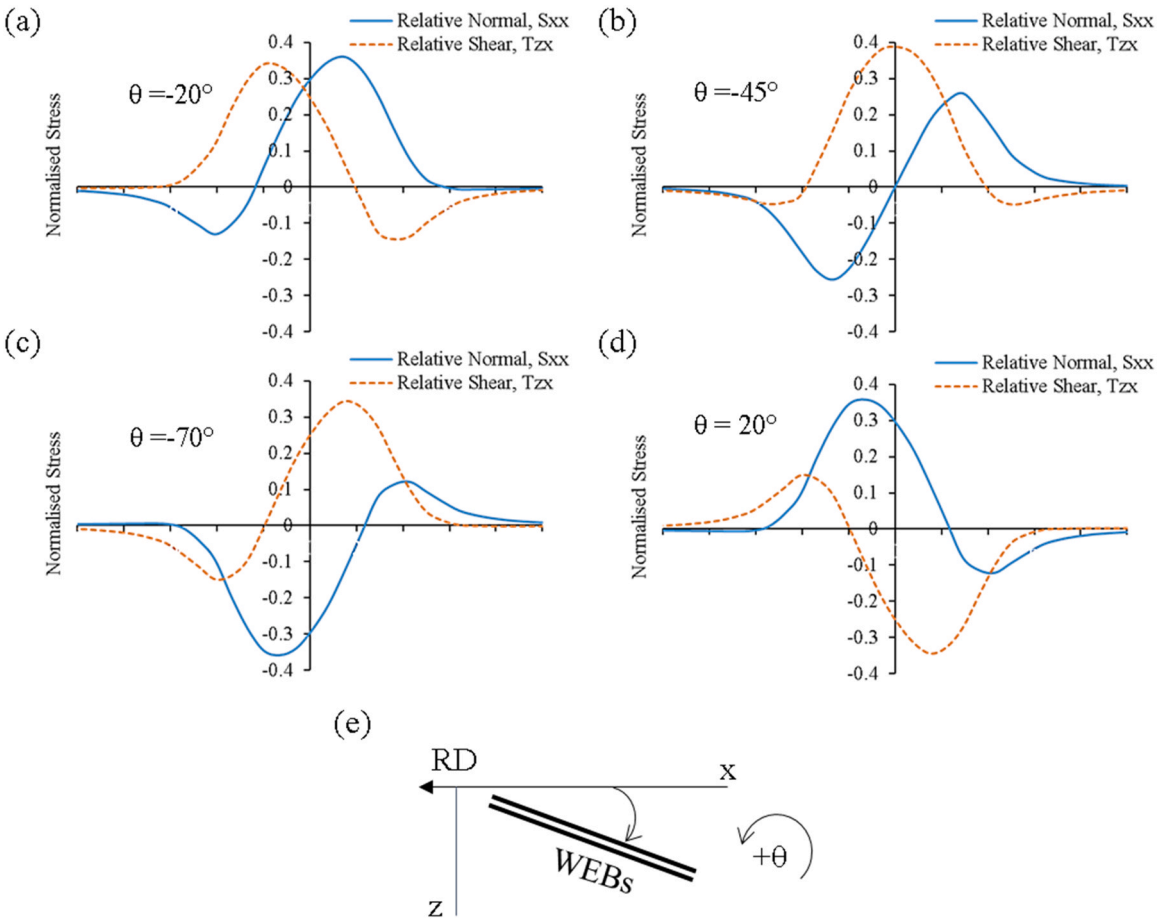

Fig. 11. Maximization of relative normal stress (S_{xx})and relative shear stress (T_{zx}) across contact path at representative depth = 0.48a, for various orientation of WEBs e.g., θ = −20°, −45°, −70°, 20° as shown in (a), (b), (c) and (d) respectively; schematic for WEBs orientation with RD is shown in (e).

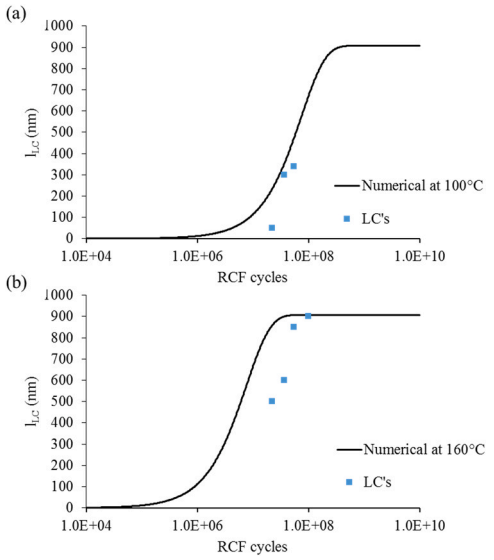

Fig. 12. (a), (b) Thickening of lenticular carbides with experimental and numerical model [15] at 100 °C and 160 °C operating temperature.

Table 4
Material properties for dislocation gliding model.

Constant	Value
A	3×10^{-30} N m^2 [30]
b	0.2876 nm [31]
D	$D_o\, e^{-E/RT}$
D_o	6.2×10^{-7} m^2 s^{-1} [32]
E	80,000 J mol^{-1} a [32]
R	8.314 J K^{-1} mol^{-1}
K_b	1.38×10^{-23} m^2 kg s^{-2} K^{-1}
C_{Vo}	2.606 at%
$C_{V\theta}$	25.79 at% [26]
λ	10 μm

WEBs growth. In order to support this argument, the growth of HABs is presented as a change in length, thickness and spacing of HABs. The characteristic growth of HABs (i.e., length, thickness, spacing) is acquired for a single band and plotted in Fig. 9 to compare with contact track plastic deformation, obtained from interferometer. From Fig. 9(a, b, c), it can be seen that the length and thickness of HABs increase rapidly up to 55 million cycles and then its growth decelerates till 100 million cycles, whereas the spacing between HABs decreases continuously. The change in characteristics length, thickness and spacing indicate that WEBs not only grow in all possible dimensions, but its density also increases with successive stress cycles. A similar trend of contact track plastic deformation can also be observed in Fig. 9(d) where the plasticity keeps on accumulating indicating the ratcheting response of the bearing material. The continuously accumulating plasticity along with the characteristic growth of HABs confirms the WEBs formation mechanism to be yield controlled.

It was suggested by Fu et al. [21] that the ferrite bands within WEBs contain dislocation cell which manifests RCF induced subsurface accumulated plastic strains. He also reported the magnitudes of accumulated plasticity in the range of 0.01863 and dislocation density of ferrite bands to be 5.69×10^{15} m^{-2}. It is evident from Fig. 9(d) that the development and growth of HABs is related with the accumulation of subsurface plasticity. An incremental change in plasticity with increasing RCF cycles is also reflected by a similar growth of WEBs.

4.2. Development of WEBs

The order of appearance for feature microstructure in current research is formation of DERs followed by the development of LABs and HABs at 100 °C operating temperature whereas at elevated temperature (160 °C) the HABs proceed LABs. Additionally, the length, thickness, spacing, structure and density of LABs, HABs and sLABs are distinct and listed in Table 3. The growth of WEBs can be seen as a function of depth and rolling cycles. Fig. 10(a) represents the centreline subsurface stress distribution, obtained from the Hertzian theory of ball-on-ball point contact, at 6 GPa maximum contact stress. Fig. 10(b) and (c) represent the gradual progression of WEBs across depth with progressive stress cycles at 100 °C and 160 °C respectively. The saturation of LABs and development of HABs on top of LABs can be observed at 100 °C just after 37 million cycles. On the other hand, at 160 °C, the HABs develop closer to the surface and grow continuously with the formation of sLABs after 55 million cycles. A qualitative analysis of WEBs growth with corresponding stress component corroborates that the formation of WEBs is strongly related to the distribution of maximum principal shear stress where the LABs initiate at higher depths and HABs along with sLABs lie closer to the surface.

It is postulated that formation of white bands is due to shear localization of bands under local micro strains which accumulate over millions of cycles and form respective ferrite bands. The formation of ferrite bands is accompanied by the dissolution of carbides leaving behind supersaturated ferrite, as indicated in Figs. 4 and 5. The shear localization and propagation with local micro strain develop a slip system in the preferred plane of WEBs causing large amount of dislocation [26]. The unceasing dislocation motion during RCF and supersaturated ferrite bands facilitate the migration of carbon atoms to form LCs. However, it is debatable why dislocation glide occurs in certain characteristic planes to form respective white bands.

Zwirlein and Schlicht [27] reported that the ferrite bands are formed due to relative normal stress, S_{xx} (also known as deviatoric stress) and relative shear stress, T_{zx}, whereas the relative stress is defined as the difference between respective stress tensor and the hydrostatic mean stress. They suggested that flat bands grow perpendicular to the relative tensile stress whereas the steeper bands grow in the direction of relative shear stress i.e., 45° to the deviatoric stresses. The effects of residual stress and traction coefficient have also been incorporated in [3,16] to explain WEBs orientation, however the proposed models requires further experimental data to support their arguments. A recent study [28] has reported that the development of WEBs requires a rolling mechanism, where reversal of stress is necessary for such microstructural alterations, hence a static subsurface stress field cannot explain the unique orientations of WEBs. It was suggested by Polonsky and Keer [12] that the physics behind the formation of WEBs can be explained with the understanding of carbon outflow from the shear bands whereas the distribution of alternating stress range determine the orientations of WEBs. They explained that during rolling cycle, a WEB is experienced by the two major extrema of alternating relative normal stress ($S_{a,xx}$) and shear stress (T_{zx}) respectively. During such non-proportional stress history, the cyclic (normal) plastic strain $\varepsilon_{p,xx}$ can be expressed in terms of alternating relative normal stress $S_{a,xx}$ and elastic stress in WEBs $S_{b,xx}$ as,

$$\varepsilon_{p,xx} = \frac{3}{2}\frac{(1-v)}{1+v}\frac{\left(S_{a,xx} - S_{b,xx}\right)}{G} \tag{1}$$

where v and G represents Poisson's ratio and plastic modulus, respectively. Eq. (1) represents that the $S_{a,xx}$ may cause a localised $\varepsilon_{p,xx}$ resulting in a residual hydrostatic pressure p_r within a WEB, which can be expressed in Eq. (2).

$$p_r = \frac{2}{3}\frac{(1+v)}{1-v} G \quad \varepsilon_{p,xx} \tag{2}$$

A $p_r > 0$ facilitates the carbon outflow from a WEB. Thus,

considering mentioned condition, criteria for LABs orientation can be expressed as it tends to adopt such orientation where a maximum of $S_{a,xx}$ exist at the end of a loading cycle and its value is as high as possible. Alternatively, the favourable orientation for HABs would be 45° to the LABs, as reported by Zwirlein and Schlicht [27]. Fig. 11 represents the maximization of relative normal stress (S_{xx}) and relative shear stress (T_{zx}) across contact path at a representative depth of 0.48a (centreline depth of maximum shear stress, where 'a' represents half-width), which have been obtained for various orientation of WEBs e.g., $\theta = -20°$, $-45°$, $-70°$, $20°$ as shown in Fig. 11(a), (b), (c) and (d) respectively. A favourable orientation for LABs lies in the vicinity of $\theta = -20°$ and its schematic is represented in Fig. 11(e) with respect to the rolling direction. Following Fig. 11 and models presented in [12,27], the unique orientation for LABs and HABs can be explained reasonably and corroborates well with the experimental data provided in the current study.

4.3. Formation mechanism

Development of WEBs can be explained by understanding carbon migration theories. During RCF loading, the ferrite bands, formed due to shear localization, lose their original plate-like microstructure and decay into a heavily deformed ferrite bands, containing high dislocation density. It is suggested that the applied shear stress along with a large hydrostatic stress cause initiation of plastic deformation resulting in dissolution of primary carbides, as observed in Fig. 4. The supersaturated regions of deformed ferrite tend to diffuse out carbon to the boundaries of ferrite band where it can be segregated in terms of lenticular carbides. The EDS analysis and nanoindentation mapping of WEBs have confirmed the carbon depletion of ferrite bands and continuous growth of lenticular carbides. However, these lenticular carbides not only grow along the boundaries of ferrite bands but form local clusters in the later stages of WEBs as discussed earlier.

It was suggested by Fu et al. [15] that the migration of carbon from the supersaturated ferrite is primarily governed by the dislocations glide. Fig. 12(a) and (b) represents thickening of LCs (I_{LC}) at 100 °C and 160 °C as obtained in current research work and compared with the numerical prediction of dislocation gliding model (details are available in Appendix). It can be seen that the growth of LCs is quite consistent with the numerical prediction at 6 GPa, 100 °C with 9100 cpm cyclic speed. However, at 160 °C operating temperature, the numerical curve slightly deviates from the current experimental data. The discrepancy of the numerical model with the experimental data can be depicted to effect of thermal diffusion of carbon at elevated temperatures. The formation mechanism for WEBs can be explained by the redistribution of carbon atoms and understanding the rearrangement of mobile dislocations within ferrite bands [6]. Formation of ferrite bands due to local shear deformation causes significant dislocations density. The strain field surrounding dislocations can attract carbon atoms which consequently gives a strong interaction between the two. The unique orientations of the WEBs arise due to the maximization of the relative normal stress along the contact track resulting in a plastic normal strain. The localised normal strain give rise to an internal hydrostatic pressure within WEBs which can influence the carbon outflow from the WEB. Additionally, RCF causes continuous dislocation gliding which can also assist the transportation of carbon atoms within the matrix. The continuous transportation of carbon towards ferrite boundaries leads to thickening of lenticular carbides. In the later stages of RCF, fully saturated HABs show the predominant formation of lenticular carbides which are formed not only along with boundaries but also within ferrite bands. The enhanced formation of LCs within HABs illustrate the role of carbon diffusion at elevated temperatures. Carbon atoms leaving the ferrite bands from the initial nucleation sites and recrystallize along the boundaries of ferrite band is supported by dislocation glide and diffusion process where thermal effects and hydrostatic pressure gradient could play a certain role. The subsequent results from 4-ball testing in comparison with theoretical models affirms the WEBs formation to be a combined effect of plasticity and carbon atoms diffusion. The extreme testing conditions as employed in current research are rarely met in nominal bearing operations except under quasi-static analysis. However, the testing load as high as 6 GPa with 100 °C (nominal) and 160 °C (close to tempering conditions) clarify the effect of thermal tempering and lowering of yield stress on WEBs formation. The understanding obtained from experimental analysis is beneficial in terms of accurately modelling the WEB formation. The previously presented dislocation gliding models [15,26] can be integrated with a more complex cyclic plasticity material model. Additionally, the WEBs can be further quantified to develop semi-empirical models for bands formation. The prognostic models based on experimental results and correct micro-mechanical response of bearing steel will be highly significant for bearing element failure.

5. Summary

- A rotary tribometer has been employed for the accelerated rolling contact fatigue (RCF) testing of standard AISI 52100 bearing balls. The post RCF investigations have been carried out to understand the formation mechanism of white etching bands (WEBs) in ball-on-ball point contact with pure-rolling cycles.
- Different feature microstructure i.e., lower angle bands, higher angle bands and secondary lower angle bands are observed in a very early stage of RCF at 6 GPa contact pressure with variation in operating temperature. The microscopic investigations have revealed that the reversal of sequence of WEBs does not depend on applied load and is strongly affected by the temperature and temperature/load combination.
- Comparison of subsurface stress field with WEBs growth indicates that white bands originate in the vicinity of maximum principal shear stresses, however their distinct orientations are governed by the maximization of relative normal stress. The WEBs tend to form at an orientation where S_{xx} is maximum along all major stress extrema along contact track.
- The characterisation of WEBs with nanoindentation mapping and EDS analysis validates the redistribution of carbon and resulting zones of hardening and softening within WEBs.
- The numerical and experimental measurement of LCs thickening illustrate that the formation of WEBs is a combined effect of plasticity and diffusion however it is still unclear how strong the influence of thermal diffusion is and require further investigations.

CRediT authorship contribution statement

The following authors have made significant contributions to this paper. Their individual contributions, not limited to, are briefly mentioned below.

Muhammad U Abdullah: Postgraduate researcher who has been conducting experimental study and numerical analysis. Major contributions to planning, scheduling of experimental work and data acquisition and analysis. He has made major contributions to writing the original manuscript. **Zulfiqar A Khan:** Principal investigator and supervisor, who led the conception of idea in terms ordinality and significance. Organized funding, resources and project management. Contributed academic critique and review of the work. **Wolfram Kruhoeffer:** Industrial advisor who have been contributing to the progress of this study in terms of deliverables. Contributed to academic critique and review of the work. **Toni Balss:** Industrial advisor who have been contributing to testing setup and guidance in sample preparation and metallography. **Bernd Vierneusel:** Industrial advisor who have provided critiques and review to the presented research work.

Declaration of Competing Interest

The authors declare that they have no known competing financial

interests or personal relationships that could have appeared to influence the work reported in this paper.

Acknowledgements

Authors would like to acknowledge Schaeffler Technologies AG & Co, KG, Germany for their direct (grant ID: 10187) and in-kind support for conducting this research at Bournemouth University, United Kingdom.

Appendix

Carbide precipitation model

The stress-induced carbide precipitation model [15] states the thickening of lenticular carbides I_{LC} as a function of cycling time $t = N/N'$, where N and N' represents stress cycles and cyclic frequency respectively. The rate of change of I_{LC} as expressed by is given as,

$$\frac{dI_{LC}}{dt}(C_{V\theta} - C_{Vb}) = \frac{\Delta\gamma N'}{b} \left[3 \left(\frac{\pi}{2}\right)^{\frac{1}{3}} \left(\frac{AD}{K_b T N'}\right)^{\frac{2}{3}} C_{Vb} \right] \tag{3}$$

Where $C_{V\theta}$ and C_{Vb} represents carbon concentration within lenticular carbides and ferrite bands, $\Delta\gamma$ represents plastic strain per stress cycle, b represents Burger vector, A represents interaction energy between carbon atoms and dislocation strain field, D represents the diffusion coefficient of carbon atoms in α ferrite, K_b represents Boltzmann constant and T is temperature in kelvin. To solve Eq. 1, C_{Vb} can be evaluated by

$$C_{Vb} = \frac{\lambda \quad C_{Vo} - I_{LC} \quad C_{V\theta}}{\lambda - I_{LC}} \tag{4}$$

Here λ shows the width of a fully developed white band and C_{Vo} represents the initial carbon concentration of the system. The material input parameters for the current study are listed in Table 4 and the plastic strain range can be obtained by Eq. 3 with the help of applied principal shear stress $\tau_{applied}$ and the shear yield limit $\tau_{y,shear}$, whose values can be obtained from classical Hertzian theory and monotonic tension/compression curve of current bearing samples [18,29].

$$\Delta\gamma = 0.0003 \quad \left(\frac{\tau_{applied}}{\tau_{y,\quad shear}} - 1\right)^3 \tag{5}$$

References

[1] Swahn H, Becker P, Vingsbo O. Martensite decay during rolling contact fatigue in ball bearings. Metall Mater Trans A 1976;7(8):1099–110.
[2] Sadeghi F, Jalalahmadi B, Slack TS, Raje N, Arakere NK. A review of rolling contact fatigue. J Tribol 2009;131(4):041403.
[3] Zwirlein O, Schlicht H. Rolling contact fatigue mechanisms—accelerated testing versus field performance, in Rolling Contact Fatigue Testing of Bearing Steels. ASTM International; 1982.
[4] Martin, J., S. Borgese, and A. Eberhardt, Microstructural alterations of rolling—bearing steel undergoing cyclic stressing. 1966.
[5] Šmeļova V, Schwedt A, Wang L, Holweger W, Mayer J. Electron microscopy investigations of microstructural alterations due to classical Rolling Contact Fatigue (RCF) in martensitic AISI 52100 bearing steel. Int J Fatigue 2017;98:142–54.
[6] El Laithy M, Wang L, Harvey TJ, Vierneusel B, Correns M, Blass T. Further understanding of rolling contact fatigue in rolling element bearings—a review. Tribol Int 2019;140:105849.
[7] Kang J. Mechanisms of microstructural damage during rolling contact fatigue of bearing steels. University of Cambridge; 2014.
[8] El Laithy M, Wang L, Harvey TJ, Vierneusel B. Re-investigation of dark etching regions and white etching bands in SAE 52100 bearing steel due to rolling contact fatigue. Int J Fatigue 2020;136:105591.
[9] Ganti, S., et al., Three-dimensional (3D) analysis of white etching bands (WEBs) in AISI M50 bearing steel using automated serial sectioning. 2018. 138: p. 11–18.
[10] Mitamura N, Hidaka H, Takaki S. Microstructural development in bearing steel during rolling contact fatigue. Materials science forum. Trans Tech Publ.; 2007.
[11] Bhargava, V., G. Hahn, and C.J.M.T.A. Rubin, Rolling contact deformation, etching effects, and failure of high-strength bearing steel. 1990. 21(7): p. 1921–1931.
[12] Polonsky I, Keer L. On white etching band formation in rolling bearings. J Mech Phys Solids 1995;43(4):637–69.
[13] Schlicht, H.J.B. and r.b. engineering, Material properties adapted to the actual stressing in a rolling bearing. 1981. 1: p. 24–29.
[14] Warhadpande A, Sadeghi F, Evans RD. Microstructural alterations in bearing steels under rolling contact fatigue: Part 2—diffusion-based modeling approach. Tribol Trans 2014;57(1):66–76.
[15] Fu H, Galindo-Nava E, Rivera-Díaz-del-Castillo P. Modelling and characterisation of stress-induced carbide precipitation in bearing steels under rolling contact fatigue. Acta Mater 2017;128:176–87.
[16] Johnson K. Formation of shear bands in ball-bearing races. University of Cambridge Department of Engineering; 1988.
[17] Barrow A, Rivera-Díaz-del-Castillo P. Nanoprecipitation in bearing steels. Acta Mater 2011;59(19):7155–67.
[18] Abdullah MU, Khan ZA, Kruhoeffer W. Evaluation of dark etching regions for standard bearing steel under accelerated rolling contact fatigue. Tribol Int 2020;152:106579.
[19] Warhadpande A, Sadeghi F, Evans RD. Microstructural alterations in bearing steels under rolling contact fatigue part 1—historical overview. Tribol Trans 2013;56(3):349–58.
[20] Zaretsky EV. Rolling bearing steels – a technical and historical perspective. Mater Sci Technol 2012;28(1):58–69.
[21] Fu H, Rivera-Díaz-del-Castillo, Pedro EJ. Evolution of white etching bands in 100Cr6 bearing steel under rolling contact-fatigue. Metals 2019;9(5):491.
[22] Kanetani, K. and K.J.M.T. Ushioda, Mechanism of white band (WB) formation due to rolling contact fatigue in carburized SAE4320 steel. 2020. 61(9): p. 1750–1759.
[23] Swahn H, Becker P, Vingsbo O. Electron-microscope studies of carbide decay during contact fatigue in ball bearings. Met Sci 1976;10(1):35–9.
[24] Voskamp A. Material response to rolling contact loading (ISSN 0742-4787) ASME Trans J Tribol 1985;107:359–64.
[25] Fu, H., Rivera-Díaz-del-Castillo, P.E.J.A.M., A unified theory for microstructural alterations in bearing steels under rolling contact fatigue, 2018, 155: p. 43–55.
[26] Kang J-H, Hosseinkhani B, Vegter RH, Rivera-Díaz-del-Castillo PEJ. Modelling dislocation assisted tempering during rolling contact fatigue in bearing steels. Int J Fatigue 2015;75:115–25.
[27] Zwirlein O, Schlicht H. Werkstoffanstrengung bei Wälzbeanspruchung–Einfluß von Reibung und Eigenspannungen. Mater Werkst 1980;11(1):1–14.
[28] Zheng X, Zhang Y, Du SJM. Preliminary research on response of GCr15 bearing steel under cyclic compression. Materials 2020;13(16):3443.
[29] Abdullah MU, Khan ZA, Kruhoeffer W, Blass T. A 3D finite element model of rolling contact fatigue for evolved material response and residual stress estimation. Tribol Lett 2020;68(4):122.
[30] Cottrell AH, Bilby B. Dislocation theory of yielding and strain ageing of iron. Proc Phys Soc Sect A 1949;62(1):49.
[31] Fu H, Song W, Galindo-Nava EI, Rivera-Díaz-del-Castillo PEJ. Strain-induced martensite decay in bearing steels under rolling contact fatigue: modelling and atomic-scale characterisation. Acta Mater 2017;139:163–73.
[32] Bhadeshia H, Honeycombe R. Steels: microstructure and properties. Butterworth-Heinemann; 2017.